Computational Insights into HVA/β-CD Inclusion Complexes: Thermodynamics, Structural Analysis, and NMR Correlations

F. Bouallag, A. Bendjeddou, H. Nouioua, T. Abbaza, A.K. Gouasmia, D. Villemin

Computational Insights into HVA/β-CD Inclusion Complexes: Thermodynamics, Structural Analysis, and NMR Correlations

F. Bouallag[a,b,*], A. Bendjeddou[a], H. Nouioua[c], T. Abbaz[a,c], A.K. Gouasmia[c] and D. Villemin[d]

[a]*Laboratory of Organic Chemistry and Interdisciplinary, University of Mohamed Cherif Messaadia, Souk Ahras, 41000, Algeria*
[b]*Laboratory of Science and Technology of Water and Environment, University of Mohamed Cherif Messaadia, Souk Ahras, 41000, Algeria*
[c]*Laboratory of Organic Materials and Heterochemistry, University of LarbiTebessi, Tébessa, 12000, Algeria*
[d]*Laboratory of Molecular and Thio-Organic Chemistry, University of Caen, Caen 14050, France*

This study employed advanced computational methods, including semi-empirical parametric method 3 (PM3) and density functional theory (DFT), to investigate the host/guest inclusion complexes of β-cyclodextrin (β-CD) with homovanilic acid (HVA). Utilizing B3LYP, M08HX, and PW6B95 approaches, global minima were optimized in both vacuum and aqueous phases. The focus spanned complexation, interaction, and deformation energies, as well as the geometry, electronic structure, and chemical reactivity of HVA during encapsulation. Natural-bonding orbital (NBO) simulations highlighted the significant role of intermolecular hydrogen interactions in the stability of HVA/β-CD complexes. The study, employing the Global-hybrid meta-GGA functional methodology (PW6B95/6-31G(d)), shed light on energetically favored molecules, emphasizing superior results in orientation A. The Gauge-Including Atomic Orbital (GIAO) method has been used to study 1H nuclear magnetic resonance (NMR) complexes. These insights contribute to advancing host-guest systems and drug delivery applications.

Keywords: β-cyclodextrin, Homovanilic acid (HVA), Density functional theory (DFT), Natural-bonding orbital (NBO), Gauge-Including Atomic Orbital

INTRODUCTION

Cyclodextrins (CDs) constitute a non-reducing class of cyclic oligosaccharides, comprised of a macrocyclic ring of glucose subunits connected by α-1,4 glycosidic linkages. These compounds are enzymatically derived from starch, typically featuring more than six glucose units [1]. Within the CD series, individual CDs possess six, seven, or eight glucose units. CDs, incorporating hydrophobic moieties of suitable dimensions, are recognized for forming inclusion complexes with a diverse array of guest substances, with the most extensively investigated complexes having a guest-host stoichiometry of 1:1 or 1:2 [2].

Homovanillic acid (HVA), the 3-O-methyl ether of (3,4-dihydroxy phenyl) acetic acid, stands as a metabolite of catecholamines. Functioning as a natural molecule with a catechol ring, it serves as a neurotransmitter or hormone in both humans and mice [3]. In addition to its correlation with dopamine levels in the brain, HVA is employed as a reagent for identifying oxidative enzymes [4]. Its presence aids in diagnosing malignant pheochromocytoma and neuroblastoma, categorizing it within the methoxy phenols family of chemical compounds. Methoxyphenols are characterized by a phenol moiety's benzene ring linked to a methoxy group. Catechol o-methyltransferase catalyzes the conversion of the deaminated metabolite of dopamine, 3,4-dihydroxyphenylacetic acid, into HVA [5]. Depression, sleep

disturbances, anxiety, and fatigue are indicative of reduced urine HVA levels. Urine testing for this metabolite proves to be a valuable method for assessing early exposure to urban pollution. HVA was selected as a model for study by Dineiro *et al.* [3], owing to its structural diversity, numerous functional groups, and clinical significance as a marker of neurotransmitter metabolism.

In cyclodextrins, encapsulation is governed by non-covalent interactions between the guest molecule (the complexed molecule) and the host molecule (β-CD, the complexing agent). Molecular modeling has proven to be instrumental in the study of inclusion complexes, enabling the exploration of geometry and the identification of various interactions between these two entities. Non-covalent intermolecular interactions play a pivotal role in supramolecular recognition and enzyme-substrate binding, making them crucial subjects for model studies on the inclusion complexes of cyclodextrins with diverse substrates [6,7]. The motivations behind complexation and the introduction of regioselectivity in cyclodextrin-catalyzed reactions can be elucidated through theoretical calculations [8-10]. Molecular mechanics (MM) computations have been predominantly employed in cyclodextrin research due to their efficiency in handling molecular size [11-15].

In this paper, a theoretical approach was presented. This investigation delved into the energy and geometry of the complexation between β-cyclodextrin and HVA, utilizing the techniques B3LYP [16], M08HX [17-20], and PW6B95 [21,22]. This comparative analysis aimed to evaluate the main intermolecular interactions between the guest and host molecules. Subsequently, natural-bonding orbital (NBO) calculations and non-covalent interaction analysis (NCI) were employed to provide detailed insights into the various interactions between hosts and guests. Finally, the chemical shift deviations obtained from Gauge-Including Atomic Orbital (GIAO) calculations was compared with the corresponding experimental values of ^{1}H NMR.

COMPUTATIONAL DETAILS

Density functional theory (DFT) calculations were conducted using three distinct functionals, namely Becke's three parameters Lee-Yang-Parr (B3LYP) [23,24], PW6B95 (a 6-parameter functional based on Perdew-Wang-91 exchange and Becke-95 correlation), and the hybrid meta-GGA functional M08HX. These calculations were executed using the basis set 6-31G(d) at the theoretical level. No constraints were imposed on the geometry during the calculations, allowing for the simulation of optimized geometric parameters, NBO analysis, and Mulliken charge distribution. Additionally, GIAO approach [25,26] was employed to investigate chemical shifts using the PW6B95/6-311+G(2d,p) and M08HX/6-311+G(2d,p) methods.

The initial geometry of β-CD and HVA was retrieved from the PubChem chemical database [27] and subsequently optimized using Gaussian 16 [28] with the PM3 semi-empirical approach [29,30]. Combining the β-CD/HVA structures was accomplished using the molecular modeling program Hyperchem 7.5 [31], and the software Gauss View 5.0.8 [32] was utilized for result visualization and processing. The host and guest structures were optimized using the PM3 approach, as illustrated in Fig. 1.

The HVA/β-CD complex was generated according to the procedure outlined in the literature [33,34]. Here, the glycosidic oxygen atoms of cyclodextrin were arranged in the XY plane, considered the center of the system coordinates. The guest molecule was positioned along the Z-axis, allowing for two orientations (Fig. 2):

- "Orientation A" where the hydroxyl group of HVA points to the broadside of the secondary hydroxylation of β-CD.
- "Orientation B" where the guest hydroxyl group points to the primary hydroxyl group of β-CD (narrow side).

The Z coordinate was employed to define the relative positions of the host and guest. The HVA guest was systematically moved to approach and traverse the β-CD cavity along the Z axis from -6 to +6, with a step size of 1. The semi-empirical PM3 approach was employed to optimize the HVA/β-CD for each step [35-37]. Subsequently, the resulting structures were re-optimized using the B3LYP/6-31G(d), M-08HX/6-31G(d), and PW6B95/6-31G(d) methods in both vacuum and aqueous phases after identifying the initial energy minima.

Using the following formulas [16], we calculated the deformation energy for each component and the interaction energy (ΔE) between the host and guest in the optimized geometries [36]:

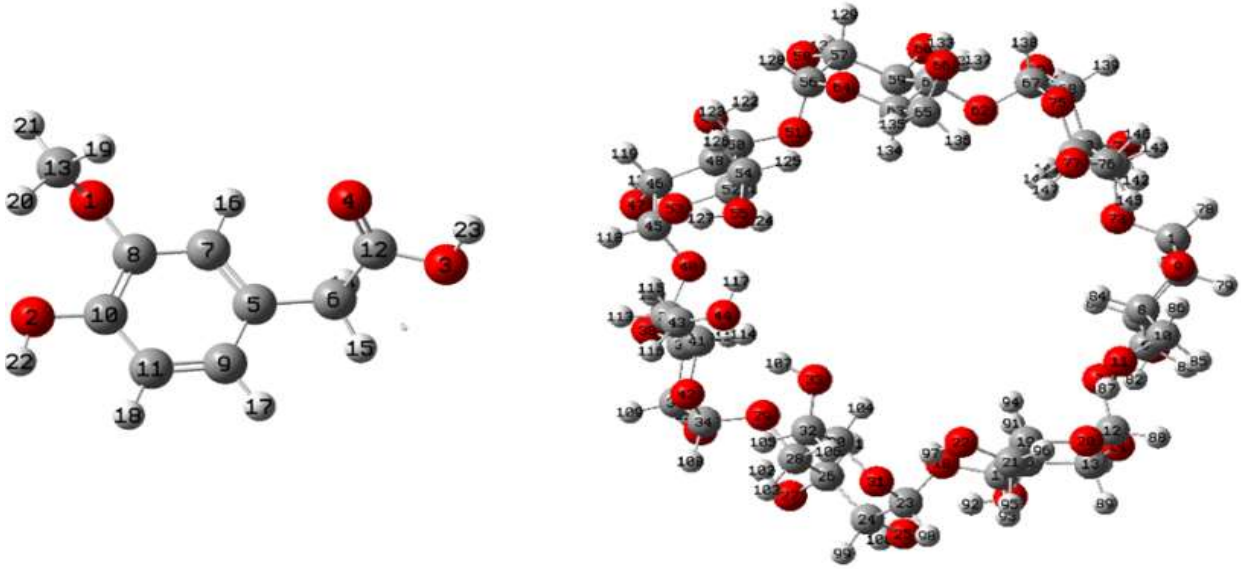

Fig. 1. The optimized host molecule (HVA) and guest molecule (β-CD) structures.

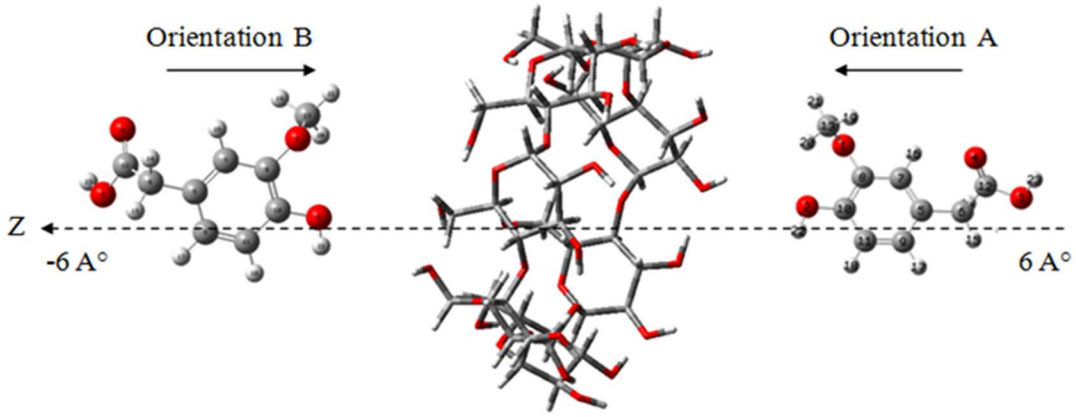

Fig. 2. Diagrammatic representation of the HVA binding mode in the β-CD cavity that creates the two orientations.

Where ($E_{complex}$) represents the total energy of the complex, ($E_{\beta CD}^{SP}$) is the single-point energy of the β-CD component using its geometry in the optimized complex, and (E_{HVA}^{SP}) is the single-point energy of the HVA component using its respective geometry in the optimized complex.

$$E_{(component)}^{DEF} = E_{SP(component)}^{OPT} - E_{(component)}^{OPT} \quad (2)$$

Where component ($E_{SP(component)}^{OPT}$) is the energy of the single point of the component using its geometry in the optimized complex, and component ($E_{(component)}^{OPT}$) is the energy of the optimized component geometry.

RESULTS AND DISCUSSION

Energies

For the HVA in β-CD, Fig. 3 illustrates the energy fluctuations of inclusion complexes as two curves. It is observed that the two stable HVA/β-CD structures were positioned at 0° for orientation A and -1° for orientation B. These structures exhibited interaction energies of -18.20 kcal mol^{-1} and -15.75 kcal mol^{-1}, respectively, with

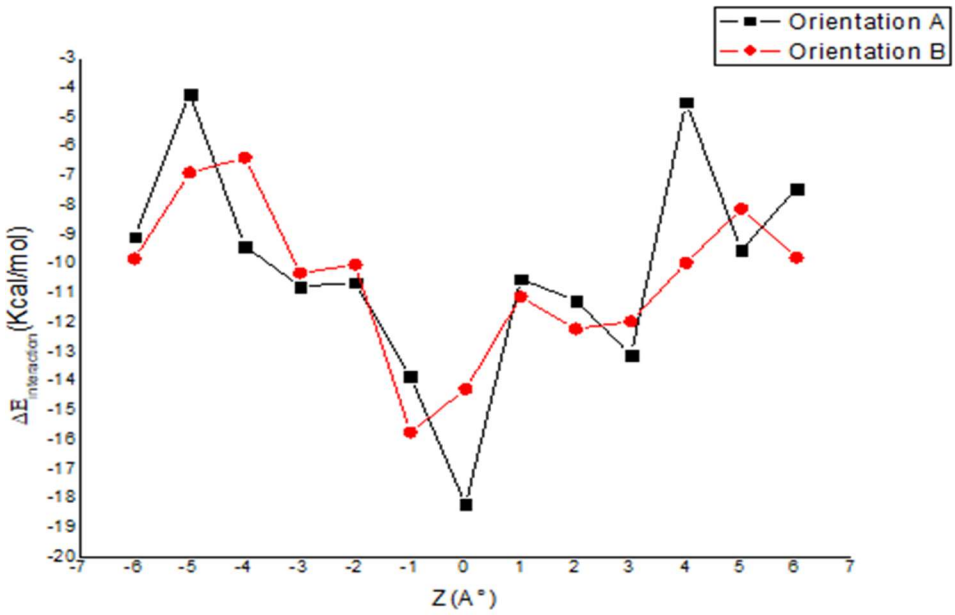

Fig. 3. PM3 estimates of the binding energies for the HVA/β-CD inclusion complexation at various locations (Z).

an energy gap of 2.45 kcal mol^{-1}. Notably, the more favorable orientation at this point was A. The negative interaction energies for both complexes indicated that the inclusion of HVA in β-CD was energetically favorable. For proper optimization of the two generated complexes at the DFT level of theory, B3LYP/6-31G(d), M-08HX/6-31G(d), and PW6B95/6-31G(d) functions were employed in both vacuum and aqueous phases. The computed energy for the most stable structures of the two orientations is summarized in Table 1.

The results extracted from Table 1 revealed that, in the vacuum phase, the interaction energy for B3LYP/6-31G(d), M08HX/6-31G(d), and PW6B95/6-31G(d) was -46.49, -47.56, and -52.37 kcal mol^{-1}, respectively, for orientation A. Conversely, for orientation B, the highest interaction energy with β-CD was observed, with values of -36.43, -49.97, and -40.79 for the respective methods. These findings consistently demonstrated that, in both vacuum and aqueous phases, the interaction in orientation A was markedly more favorable than in orientation B, aligning with earlier PM3 approach results [16]. Notably, the PW6B95/6-31G(d) method in a vacuum for orientation A yielded the highest interaction energy values. It is conventionally preferred that the complex with the most negative interaction energy is considered more stable [30]. The vacuum and aqueous phase results suggest that M08HX/6-31G(d) and PW6B95/6-31G(d) functions predict more stable geometrical structures compared to the traditional B3LYP technique.

The deformation energy analysis presented in Table 1, for both vacuum and aqueous phases, underscored that the β-CD molecule exhibited superior deformation energy compared to the HVA molecule in both orientations across all functions. Post-complexation, the flexibility of the β-CD structure emerged as a crucial factor influencing intermolecular interaction and system stability. The energy required to alter the system of an HVA molecule for bonding inside the β-CD cavity was higher for an A-orientation HVA molecule than for a B-orientation HVA molecule. These findings suggest that the formation of inclusion complexes is influenced by multiple factors, including the deformation energy of β-CD.

In the proposed favorable structures, illustrated in Fig. 4, it is evident that HVA is entirely encapsulated in the β-CD cavity for orientation A, as indicated by consistent results across all B3LYP/6-31G(d), M08HX/6-31G(d), and PW6B95/6-31G(d) functions for the two orientations.

Geometrical Parameters

The inclusion complexes in orientation A exhibited total penetration compared to orientation B in both vacuum and

Table 1. Interaction and Deformation Energies in Vacuum and Aqueous Phases (kcal mol^{-1}) for Both Orientations

	Vacuum phase		Aqueous phase	
	Orientation A	Orientation B	Orientation A	Orientation B
B3LYP/6-31G(d)				
$\Delta E_{interaction}$	-46.49	-36.43	-30.07	-24.39
E_{DEF} (β-CD)	17.71	11.06	12.11	6.71
E_{DEF} (HVA)	3.61	3.44	3.63	3.16
M08HX 6-31G(d)				
$\Delta E_{interaction}$	-47.56	-49.97	-42.34	-26.37
E_{DEF} (β-CD)	12.11	9.30	13.37	-3.37
E_{DEF} (HVA)	2.55	3.21	2.88	2.52
PW6B95 6-31G(d)				
$\Delta E_{interaction}$	-52.37	-40.79	-39.52	-29.50
E_{DEF} (β-CD)	22.89	14.67	11.68	6.59
E_{DEF} (HVA)	3.37	3.23	3.42	2.61

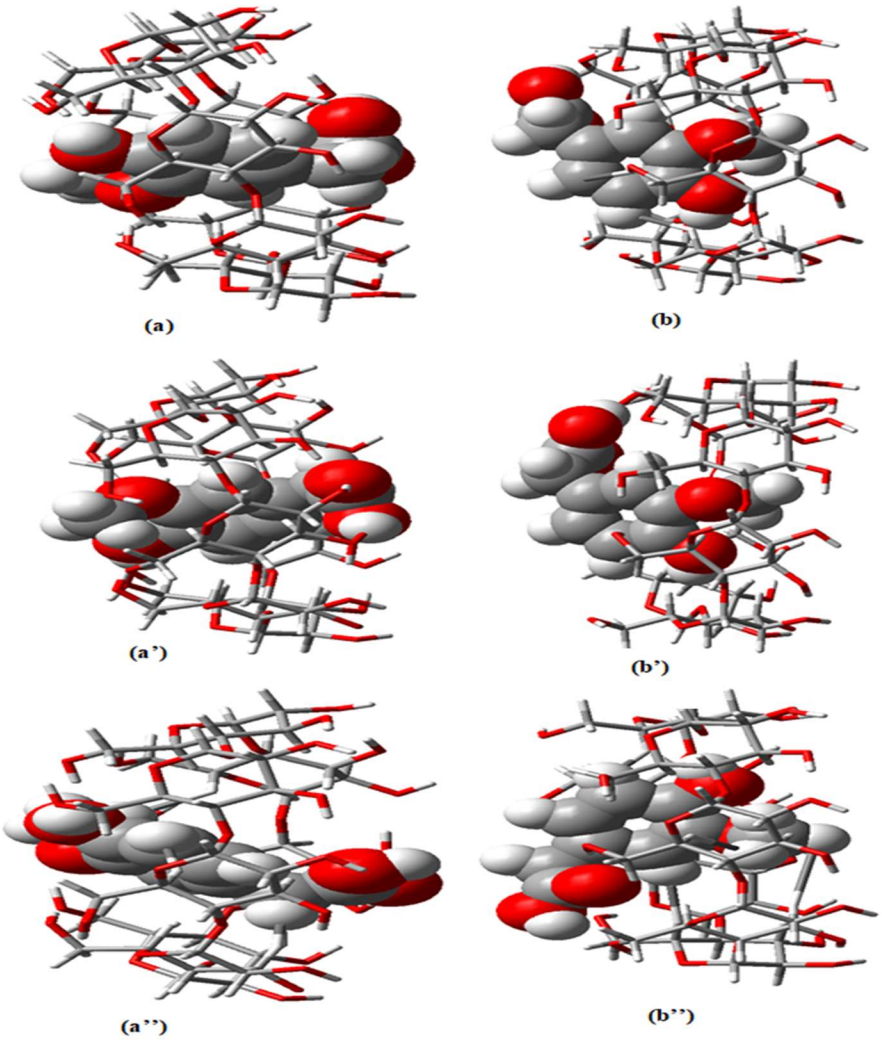

Fig. 4. Geometric structures of the most stable complexes obtained from B3LYP/6-31G(d) (a, b), M08HX/6-31G(d) (a', b'), and PW6B95/6-31G(d) (a", b") calculations for HVA/β-CD, respectively, in vacuum.

aqueous phases, based on geometric metrics. The benzene ring is fully integrated into the β-CD cavity in both orientations [37-40]. The complex geometries observed in the aqueous phase closely resemble those in the vacuum.

Tables 2, 3, and Fig. 4 summarize the optimal structural parameters (bond lengths, angles, and dihedral angles) of the HVA molecule before and after complexation as determined by the B3LYP/6-31G(d), M08HX/6-31G(d), and PW6B95/6-31G(d) theory levels in a vacuum phase.

The results indicated a significant change in the basic geometry of HVA in the complexes. This alteration was elucidated by differences in bond length, bond angle, and dihedral angle values. Notably, the dihedral angle O_{151}-C_{159}-C_{153}-C_{152} (-2.83/-7.26/-10.87°) of the free HVA molecule compared to the dihedral angle O_{151}-C_{159}-C_{153}-C_{152} (-107.50/-137.06/-105.61°) of HVA in the complex was particularly pronounced for orientation A.

In contrast, orientation B exhibited dihedral angles O_{151}-C_{159}-C_{153}-C_{152} (68.31/11.38/29.09°), and the preceding discrepancy was more noticeable. Bond angles also undergo significant distortion. The formation of a stable inclusion complex in orientation A under vacuum conditions was evident from the specific conformation adopted by HVA inside the host cavity.

Table 3 presents the geometric characteristics of β-CD before and after complexation with HVA (primary and secondary hydroxyls). Notably, interactions between the host and guest resulted in a substantial modification of the host cavity

Table 2. Geometric Parameters (Bonds, Bond Angles, and Dihedral Angles) of HVA before and after Inclusion in β-CD Calculated with B3LYP/6-31G(d) M08HX/6-31G(d) and PW6B95/6-31G(d)

	HVA_{Free}	Orientation A	Orientation B
		Bond (Å)	
O_{149}-H_{169}	0.97/0.97/0.96	0.99/0.98/0.98	0.98/0.97/0.97
O_{148}-C_{160}	1.43/1.42/1.42	1.45/1.43/1.44	1.44/1.43/1.43
O_{148}-C_{155}	1.38/1.37/1.37	1.38/1.37/1.37	1.38/1.37/1.37
O_{149}-C_{157}	1.37/1.36/1.36	1.37/1.36/1.36	1.37/1.36/1.36
O_{151}-C_{159}	1.21/1.20/1.21	1.23/1.22/1.22	1.23/1.22/1.22
O_{150}-C_{159}	1.35/1.34/1.34	1.33/1.33/1.32	1.33/1.32/1.32
O_{150}-H_{170}	0.98/0.97/0.97	1.00/0.97/0.01	1.01/0.99/0.99
		Bond angles (°)	
O_{150}-C_{159}-O_{151}	122.70/122.80/122.72	123.89/122.36/123.91	122.99/122.45/122.72
C_{159}-O_{150}-H_{170}	107.14/107.87/107.19	110.90/108.55/110.42	110.38/107.19/108.57
C_{153}-C_{159}-O_{151}	126.60/126.30/126.51	122.82/123.82/122.87	124.26/124.76/124.64
O_{150}-C_{159}-C_{153}	110.70/110.88/110.77	113.20/113.80/113.70	112.69/112.79/112.63
C_{157}-O_{149}-H_{169}	109.04/109.43/108.90	112.20/110.14/111.15	111.17/112.29/111.47
C_{155}-O_{148}-C_{160}	114.96/113.12/114.19	119.04/113.47/117.25	114.89/111.88/113.59
C_{155}-C_{157}-O_{149}	117.55/117.12/117.33	118.66/118.62/118.20	117.60/115.84/116.83
C_{157}-C_{155}-O_{148}	120.92/120.00/120.44	123.01/119.86/121.69	120.31/119.03/119.94
		Dihedral angle (°)	
O_{149}-C_{157}-C_{155}-O_{148}	-2.01/-0.99/-1.46	-6.51/-7.40/-5.43	-5.69/2.83/-3.56
C_{160}-O_{148}-C_{155}-C_{157}	73.77/74.65/73.68	53.02/87.23/58.22	77.70/77.65/78.75
O_{151}-C_{159}-O_{150}-H_{170}	-0.14/-0.36/-0.58	9.55/0.28/8.08	-7.02/-12.29/-10.42
O_{151}-C_{159}-C_{153}-C_{152}	-2.83/-7.26/-10.87	-107.50/-137.06/-105.61	68.31/11.38/29.09
O_{150}-C_{159}-C_{153}-C_{152}	177.44/173.63/170.28	69.26/44.74/70.47	-108.99/-167.75/-150.28

compared to the free β-CD. An important observation is the transformation of the round cavity of β-CD to an oval cavity following guest insertion [36]. The favorable structures, presented with PW6B95/6-31G(d) calculations for all inclusion complexes analyzed in Fig. 5, demonstrate that HVA is absorbed in the β-CD cavity through hydrogen bonds formed between the guest and the hydroxyl groups of β-CD [41,42].

Table 3. Geometric Parameters Free β-CD and Complexed Forms Calculated with B3LYP/6-31G(d) M08HX/6-31G(d) and PW6B95/6-31G(d)

	Free β-CD	Orientation A	Orientation B
Primary hydroxyls			
O_{11}-O_{22}	4.316/4.124/ 2.879	5.725/5.944/5.735	4.490/4.109/4.35
O_{22}-O_{33}	2.801/3.889/ 2.896	3.919/4.124/3.736	3.185/3.659/3.603
O_{33}-O_{44}	2.909/2.791/ 2.910	3.230/2.757/3.300	2.958/2.682/2.744
O_{44}-O_{55}	2.920/2.873/ 2.844	3.545/3.707/3.652	4.460/3.877/4.164
O_{55}-O_{66}	6.637/6.647/ 6.507	6.047/5.867/6.025	7.175/6.301/6.612
O_{66}-O_{77}	3.007/2.979/ 3.889	4.113/3.926/4.287	3.706/3.812/3.777
O_{77}-O_{11}	5.434/5.164/ 5.537	2.940/2.918/2.938	5.719/5.374/5.468
Secondary hydroxyls			
O_{36}-O_{27}	3.113/2.892/ 3.061	2.883/2.908/2.872	3.150/2.894/2.890
O_{27}-O_{25}	2.829/2.779/ 2.822	2.867/2.808/2.849	2.793/2.776/2.747
O_{25}-O_{16}	2.900/2.835/ 3.046	2.808/2.902/2.794	2.829/2.834/2.806
O_{16}-O_{14}	2.815/2.760/ 2.825	2.778/2.822/2.753	2.780/2.767/2.734
O_{14}-O_{5}	2.915/2.870/ 3.078	2.814/2.717/2.823	2.855/2.862/2.839
O_{5}-O_{3}	2.830/2.791/ 2.827	2.820/2.779/2.778	2.763/2.763/2.740
O_{3}-O_{71}	2.942/2.939/ 3.099	3.085/3.119/3.008	2.809/2.861/2.846
O_{71}-O_{69}	2.833/2.802/ 2.804	2.852/2.842/2.813	2.796/2.799/2.770
O_{69}-O_{60}	2.918/2.907/ 2.968	3.011/3.051/3.025	2.961/2.975/2.970
O_{60}-O_{58}	2.794/2.807/ 2.788	2.822/2.841/2.798	2.789/2.811/2.779
O_{58}-O_{49}	2.844/2.907/ 2.877	2.889/2.936/2.891	2.817/2.923/2.880
O_{49}-O_{47}	2.824/2.825/ 2.786	2.822/2.802/2.778	2.772/2.796/2.765
O_{47}-O_{38}	3.020/3.036/ 2.966	2.955/2.914/2.928	2.827/2.885/2.850
O_{38}-O_{36}	2.859/2.799/ 2.823	3.771/2.801/2.800	2.822/2.791/2.760
Glycosidic oxygen			
O_{29}-O_{40}	4.393/4.350/ 4.378	4.514/4.314/4.447	4.494/4.450/4.439
O_{40}-O_{51}	4.412/ 4.262/ 4.333	4.310/4.355/4.285	4.241/4.161/4.127
O_{51}-O_{62}	4.536/4.457/ 4.471	4.484/4.508/4.386	4.605/4.443/4.524
O_{62}-O_{73}	4.323/4.365/ 4.368	4.478/4.382/4.428	4.439/4.497/4.473
O_{73}-O_{7}	4.305/4.307/ 4.422	4.5414/4.239/4.483	4.324/4.328/4.298
O_{7}-O_{18}	4.552/4.374/ 4.470	4.196/4.495/4.124	4.475/4.267/4.324
O_{18}-O_{29}	4.438/4.374/4.460	4.487/4.311/4.373	4.529/4.483/4.482

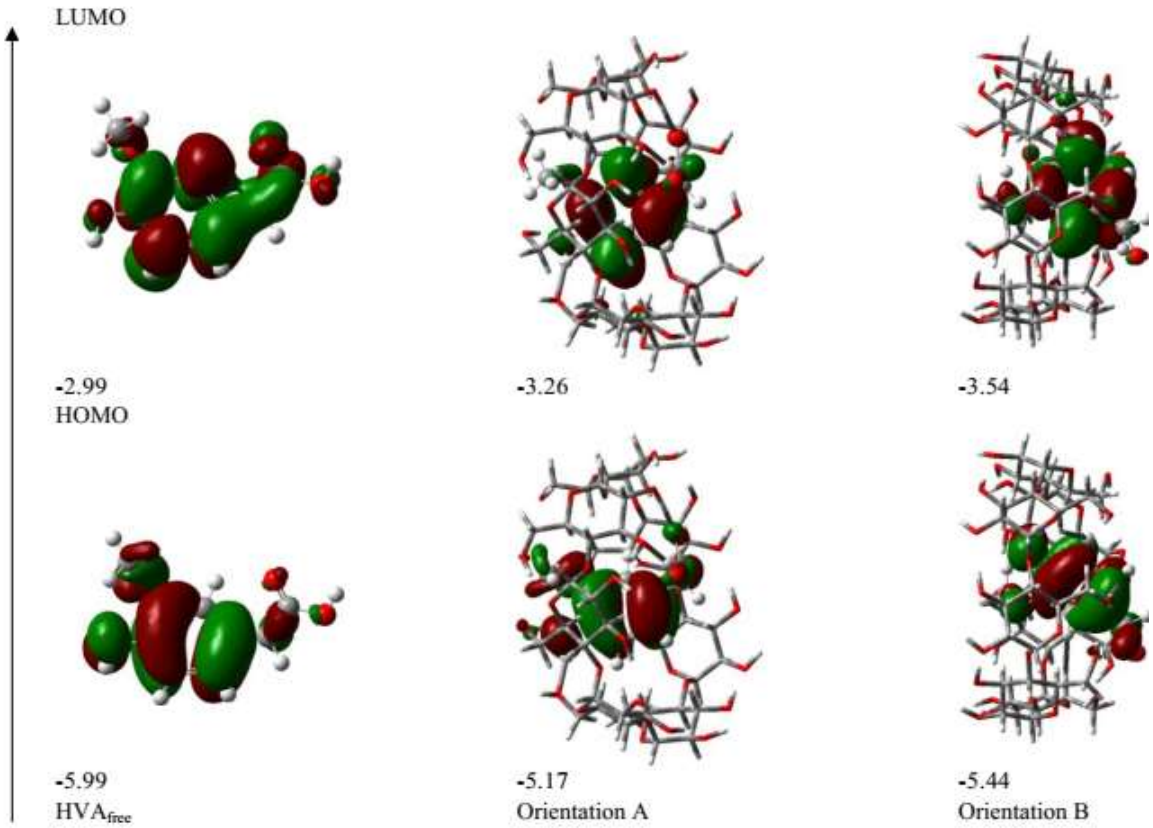

Fig. 5. HOMO and LUMO boundary molecular orbital energies for free HVA and complexed in β-CD obtained at PW6B95/6-31G(d) in vacuum.

Thermodynamic Parameters

PW6B95/6-31G(d) performed the process at 1 atmosphere and 298.15 K in both vacuum and aqueous phases for both orientations to calculate the thermodynamic parameters of the inclusion. Table 4 provides a summary of these parameters, including enthalpy change (ΔH°), Gibbs free energy (ΔG°), and entropy change (ΔS°).

According to the experimental results, the complexation reactions of HVA with β-CD are exothermic, as indicated by the negative enthalpy changes (ΔH° = -48.35 kcal mol^{-1}). Additionally, both orientations (A and B) exhibited similarly negative entropy changes (ΔS°), suggesting that the creation of the complex is now driven by enthalpy. Furthermore, the negative enthalpy variations imply that both inclusion methods are enthalpically favorable. Both complexation reactions exhibited negative ΔG° values, indicating spontaneous processes [43], and binding interactions were considered the preferred type of complexation. The negative G, H, and S values collectively suggest that the production of β-CD/HVA inclusion complexes was an enthalpy-driven process. In contrast to orientation B, the enthalpy change of orientation A (ΔH° = -48.35 kcal mol^{-1}) is more negative than that of orientation B (ΔH° = -44.71 kcal mol^{-1}). Complex A has a negative ΔH° value, signifying a strong interaction between HVA and the β-CD cavity. This is attributed to increased van der Waals interactions in both vacuum and aqueous phases [36].

Frontier Molecular Orbitals (FMO) and Chemical Reactivity

The PW6B95/6-31G(d) approach was employed to assess the chemical reactivity and site selectivity of molecular systems. The boundary molecular orbital energies, E_{HOMO} (as ionization energy) and E_{LUMO} (as electron affinity), were used to calculate the global reactivity descriptors, including electronegativity (χ), potential (μ), global hardness (η), and electrophilicity index (ω). The results were determined using Eqs. (3)-(5).

Table 4. Thermodynamic Parameters, Including HOMO, LUMO, ($E_{HOMO} - E_{LUMO}$), Electronegativity (χ), Potential (μ), Global Hardness (η), and Electrophilicity Index (ω), Estimated by PW6B95/6-31G(d) for Inclusion Complexes, HVA, and β-CD in the Vacuum and Aqueous Phases

Vacuum phase				
	β-CD free	AZ free	Orientation A	Orientation B
ΔH° (kcal mol^{-1})	-	-	-48.35	-44.71
ΔG° (kcal mol^{-1})	-	-	-32.97	-26.43
ΔS° (cal mol^{-1} K^{-1})	-	-	-52.81	-59.04
HOMO (eV)	5.17	-5.99	-5.17	-5.44
LUMO (eV)	0.27	-2.99	-3.26	-3.54
Δ ($E_{HOMO} - E_{LUMO}$)	-5.44	-3.00	-1.91	-1.9
μ (eV)	-2.45	-4.49	-4.21	-4.49
χ (eV)	2.45	4.49	4.21	4.49
η (eV)	2.72	1.5	0.96	0.95
ω (eV)	1.10	6.72	9.23	10.61
Aqueous phase				
	β-CD free	AZ free	Orientation A	Orientation B
ΔH° (kcal mol^{-1})	-	-	-39.25	-36.29
ΔG° (kcal mol^{-1})	-	-	-18.84	-16.76
ΔS° (cal mol^{-1} K^{-1})	-	-	-66.23	-65.52
HOMO (eV)	-5.44	-9.52/-6.26	-5.44	-5.44
LUMO (eV)	0.27	-0.54/-4.62	-3.54	-3.54
Δ($E_{HOMO} - E_{LUMO}$)	-5.71	-1.64	-1.9	-1.9
μ (eV)	-2.58	-5.44	-4.49	-4.49
χ (eV)	2.58	5.44	4.49	4.49
η (eV)	2.86	0.82	0.95	0.95
ω (eV)	1.16	18.04	10.61	10.61

$$\chi = -\mu = (E_{HOMO} + E_{LUMO})/2 \quad (3)$$

$$\eta = (E_{LUMO} - E_{HOMO})/2 \quad (4)$$

$$\omega = \mu^2/2\eta \quad (5)$$

Table 4 summarizes the HOMO and LUMO energies, as well as structural parameters μ, χ, η, and ω, for free HVA, β-CD, and their inclusion complexes calculated using PW6B95/6-31G(d). In this context, LUMO represents the ability to accept an electron, while HOMO represents the ability to donate electrons. The HOMO-LUMO gap, defined as ($E_{HOMO} - E_{LUMO}$), is a significant stability scale, with chemicals having higher gap values generally exhibiting greater stability [44].

In both vacuum and aqueous phases, the ($E_{HOMO} - E_{LUMO}$) gaps for complexes A (-8.17 (eV)) and B (-8.07 (eV)) were found to be convergent. Specifically, the ($E_{HOMO} - E_{LUMO}$) energy band gap obtained with PW6B95/6-31G (d) in the vacuum and aqueous phases was -1.91 (eV) for the A orientation and -1.9 (eV) for the B orientation, showing no significant difference between the two environments. Figure 5 illustrates typical HOMO and LUMO structures, revealing high electron density concentration in the benzene ring and carboxyl group for the HOMO distribution in the free state. The LUMO orbital

exhibited a distribution of low electron densities in the hydroxyl group. Importantly, the diagram indicates that the guest molecule remains entirely confined to the HOMO and LUMO orbitals in both orientations, suggesting that encapsulation does not alter the charge distribution of the guest molecule [35]. In terms of overall indices, the electron chemical potential (μ), hardness (η), electronegativity (χ), and electrophilicity (ω) values of the complexes differ from those of the individual host and guest molecules. The electronegativity (χ) of electrons increases upon conjoining the HVA molecule and β-CD. However, until the chemical electron potentials (μ) are equal, electrons are transferred to the lower chemical electron potential [45].

All inclusion complexes exhibited negative chemical potentials, indicating that the inclusion processes are spontaneous. In comparison to free β-CD, free HVA had lower chemical potential values, suggesting charge transfer from β-CD to HVA during complex formation in both orientations. The chemical hardness (η) values for both orientations in PW6B95/6-31G(d) computations in the gas phase (and in the aqueous phase) were the same at 0.0001. High values of this significant electrophilicity index are indicative of the majority of electrophilic systems [46]. The electrophilicity (ω) of orientation A in the vacuum phase (and in the aqueous phase) was determined to be 9.23 (eV) (10.61 (eV)), significantly lower than the electrophilicity of orientation B, which was calculated to be 10.61 (eV) (10.61 (eV)). This disparity suggests that complex B is more electrophilic, emphasizing the crucial role of charge transfer interactions in the stabilization of inclusion complexes. The results further indicate that the stability of the complexes is lower than that of isolated β-CD, as HVA molecules exhibit reduced hardness (η), measuring 1.5 (eV) (0.96 (eV)) when they enter the cavity of β-CD in vacuum phase orientation A.

Mulliken Charge

When applying quantum chemical calculations to such a system, the Mulliken atomic charge calculation becomes crucial. The Mulliken population [47] is a fundamental aspect in representing the charge distribution in the simplest possible way, rendering atomic populations in the molecule "sharp" due to the Mulliken charges. These charges significantly impact the dipole moment, polarizability, and electronic structure of molecules [48].

The Natural Bond Orbital (NBO) Analysis

The study of intra- and intermolecular bonding, interactions between bonds, as well as charge transfer or conjugative interaction in molecular systems, can be efficiently performed using orbital analysis of natural bonds. In this section, the mutual interactions between the two molecules were explored using the M08-HX/6-31G(d) and PW6B95/6-31G(d) levels of theory for both vacuum and aqueous orientations. Lone pairs (LP) of oxygen atoms acting as donors and OH bonds acting as acceptors lead to the most significant interactions.

Tables 6 and 7 provide their corresponding $E^{(2)}$ energies for the two orientations, with values increasing as hydrogen bonding lengths shorten (O...H). Figures 6 and 7 display numerous potent hydrogen bonds in the complexes' optimized structures, specifically for orientation A.

The significant hydrogen bonds were discovered in a vacuum when the HVA was considered as a donor.

For orientation A. (I) The first hydrogen bond was formed between the O_{44}-H_{117} bond (2.35 Å) and the hydrogen atom (H_{117}) of the O_{149}-H_{169} bond, with estimated energies of 0.23 kcal mol^{-1} (M08HX/6-31G(d)) and 0.24 kcal mol^{-1} (PW6B95/6-31G(d)).

(II) The second hydrogen bond occurred between the hydrogen atom (H_{87}) and the lone pair oxygen atom (O_{148}) of the O_{11}-H_{87} bond, positioned at 1.91 and 1.89 Å. The calculated H-bond energies were 6.11 (kcal mol^{-1}) (M08HX/6-31G(d)) and 9.42 (kcal mol^{-1}) (PW6B95/6-31G(d)).

For orientation B. (I) The first hydrogen bond, at distances of 2.30 and 2.29 Å, was between the O_{149}-H_{169} bond and the hydrogen atom (H_{121}), with $E^{(2)}$ energies of 0.33 kcal mol^{-1} (M08HX/6-31G(d)) and 0.36 kcal mol^{-1} (PW6B95/6-31G(d)).

(II) The second hydrogen bond was formed between the hydrogen atom (H_{147}) and the lone pair oxygen atom (O_{151}) in the O_{77}-H_{147} bond, positioned at 1.95 Å. The estimated H-bond energies were 4.28 (kcal mol^{-1}) (M08HX/6-31G(d)) and 5.72 kcal mol^{-1} (PW6B95/6-31G(d)).

An important hydrogen bond was identified between the lone pair (LP) (O_{55}) and $\sigma^*(O_{149}$-$H_{169})$ at 1.85 Å, with energies of 15.36 kcal mol^{-1} (M08HX/6-31G(d)) and 13.79 kcal mol^{-1} (PW6B95/6-31G(d)) when HVA acted as an acceptor. Another hydrogen bond was formed between the

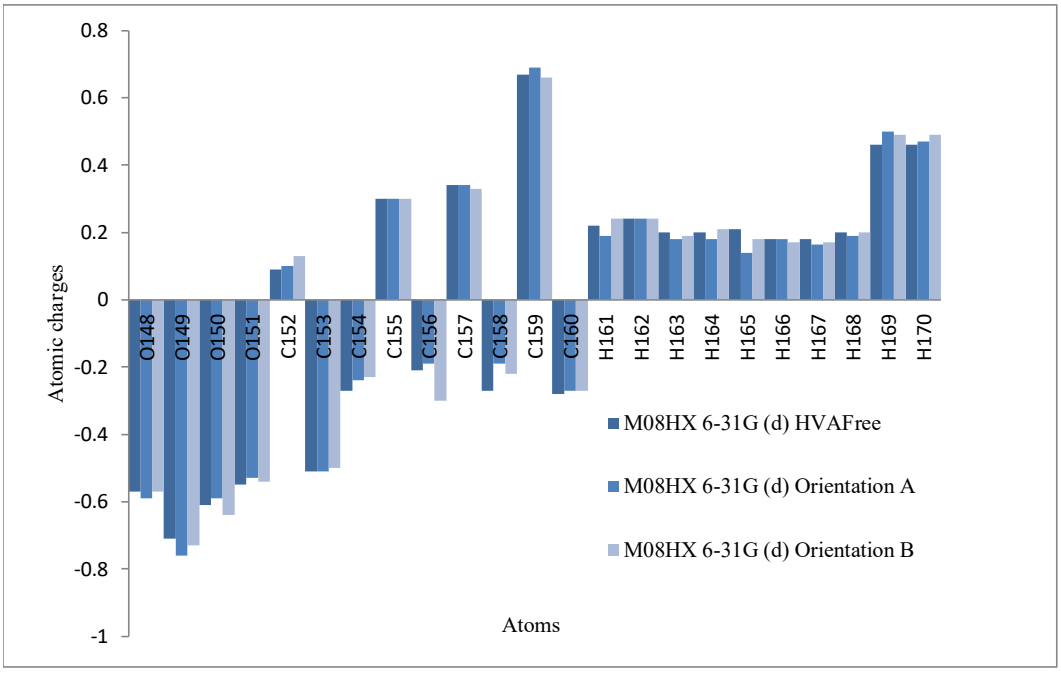

Fig. 6. Mulliken charge analysis of HVA.

Table 5. Mulliken Atomic Charges of HVA before and after Inclusion in β-CD Computed in the Aqueous Phase Using M08HX/6-31G(d), and PW6B95/6-31G(d)

	M08HX/6-31G(d)			PW6B95/6-31G(d)		
	HVA_{Free}	Orientation A	Orientation B	HVA_{Free}	Orientation A	Orientation B
O_{148}	-0.57	-0.59	-0.57	-0.56	-0.57	-0.54
O_{149}	-0.71	-0.76	-0.73	-0.67	-0.71	-0.71
O_{150}	-0.61	-0.59	-0.64	-0.56	-0.60	-0.60
O_{151}	-0.55	-0.53	-0.54	-0.52	-0.51	-0.52
C_{152}	0.09	0.10	0.13	0.09	0.09	0.13
C_{153}	-0.51	-0.51	-0.50	-0.42	-0.43	-0.48
C_{154}	-0.27	-0.24	-0.23	-0.23	-0.22	-0.21
C_{155}	0.30	0.30	0.30	0.31	0.31	0.29
C_{156}	-0.21	-0.19	-0.30	-0.20	-0.21	-0.24
C_{157}	0.34	0.34	0.33	0.32	0.32	0.32
C_{158}	-0.27	-0.19	-0.22	-0.23	-0.21	-0.22
C_{159}	0.67	0.69	0.66	0.59	0.61	0.61
C_{160}	-0.28	-0.27	-0.27	-0.23	-0.26	-0.24
H_{161}	0.22	0.19	0.24	0.20	0.21	0.22
H_{162}	0.24	0.24	0.24	0.20	0.21	0.22
H_{163}	0.20	0.18	0.19	0.16	0.18	0.17
H_{164}	0.20	0.18	0.21	0.16	0.18	0.18
H_{165}	0.21	0.14	0.18	0.17	0.16	0.17
H_{166}	0.18	0.18	0.17	0.17	0.17	0.16
H_{167}	0.18	0.164	0.17	0.17	0.18	0.17
H_{168}	0.20	0.19	0.20	0.18	0.20	0.18
H_{169}	0.46	0.50	0.49	0.45	0.47	0.47
H_{170}	0.46	0.47	0.49	0.45	0.47	0.48

Table 6. Donor-acceptor Interactions and Stabilization Energies $E^{(2)}$ (kcal mol^{-1}) of HVA/β-CD Orientation A

		Orientation A							
		Vacuum				Aqueous			
Donor	Acceptor	M-08HX		PW6B95		M-08HX		PW6B95	
		$E^{(2)}$	d (Å)	$E^{(2)}$	d (Å)	$E^{(2)}$	d (Å)	$E^{(2)}$	d (Å)
O_{149}-H_{169}	H_{117}	0.23	2.35	0.24	2.33	0.13	2.30	0.25	2.32
LP (O_7)	C_{154}-H_{163}	3.32	2.26	0.13	3.06	1.58	2.45	0.13	3.06
LP (O_{55})	O_{149}-H_{169}	15.36	1.85	13.79	1.86	3.83	1.83	15.99	1.84
LP (O_{148})	O_{11}-H_{87}	6.11	1.91	9.42	1.89	8.50	1.96	10.27	1.88

Table 7. Donor-acceptor Interactions and Stabilization Energies $E^{(2)}$ (kcal mol^{-1}) of HVA/β-CD in Orientation B

		Orientation B							
		Vacuum				Aqueous			
Donor	Acceptor	M-08HX		PW6B95		M-08HX		PW6B95	
		$E^{(2}$	d(Å)	$E^{(2)}$	d(Å)	$E^{(2)}$	d(Å)	$E^{(2)}$	d(Å)
O_{149}-H_{169}	H_{121}	0.33	2.30	0.36	2.29	0.37	2.28	0.38	2.27
LP(O_{11})	O_{150}-H_{170}	19.69	1.78	22.32	1.74	22.72	1.74	27.96	1.68
LP (O_{22})	C_{153}-H_{161}	1.81	2.47	0.89	2.66	2.01	2.42	0.50	2.83
LP (O_{51})	O_{149}-H_{169}	9.04	1.85	9.28	1.88	9.74	1.84	10.05	1.87
LP (O_{151})	O_{77}-H_{147}	4.28	1.95	5.72	1.93	5.25	1.93	6.60	1.92

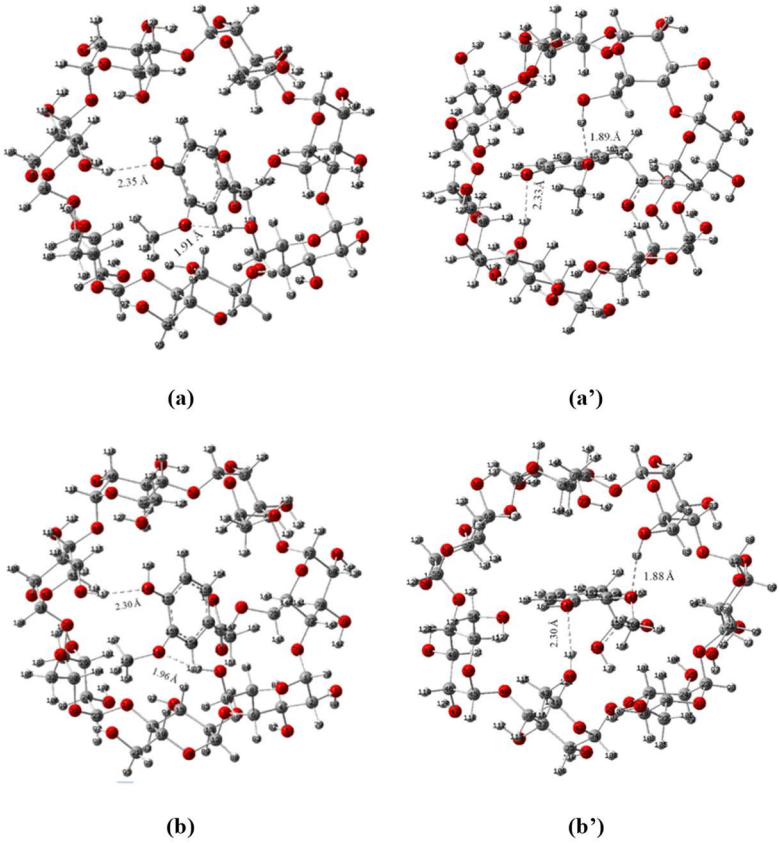

Fig. 7. Strong hydrogen bonding in Orientation A for (a) and (b) for M-08HX/6-31G(d) in vacuum and aqueous, (a') and (b') for PW6B95/6-31G(d) in vacuum and aqueous.

C_{154}-H_{163} bond and the lone pair (LP) (O_7) at distances of 1.89 and 1.91 Å, with energies of 3.32 (kcal mol^{-1}) (M08HX/6-31G(d)) and 0.13 (kcal mol^{-1}) (PW6B95/6-31G(d)).

When HVA acted as the acceptor in orientation B, (I) the initial interaction between LP (O_{11}) and σ*(O_{150}-H_{170}) was substantial, with H-bond energies of 19.69 (kcal mol^{-1}) (M08HX/6-31G(d)) and 22.32 (kcal mol^{-1}) (PW6B95/6-31G(d)) at distances of 1.95 and 1.93 Å, respectively. (II) The second hydrogen bond involved the lone pair (LP) (O_{51}) and O_{149}-H_{169} at 1.85 Å, with energies of 9.04 (kcal mol^{-1}) (M08HX/6-31G(d)) and 9.28 (kcal mol^{-1}) (PW6B95/6-31G(d)).

(III) The third hydrogen bond was formed between the lone pair oxygen atom (LP) (O_{22}) and the C_{153}-H_{161} bond at distances ranging from 2.47 to 2.66 Å, with energies of 1.81 (kcal mol^{-1}) (M08HX/6-31G(d)) and 0.89 (kcal mol^{-1} (PW6B95/6-31G(d)).

In an aqueous environment, a crucial intermolecular hydrogen bond was observed when HVA acted as the donor.

For orientation A. (I) The energy of the first hydrogen bond was calculated to be 0.13 (kcal mol^{-1}) using M08-HX/6-31G(d), and the second hydrogen bond was estimated to be 0.25 (kcal mol^{-1}) using PW6B95/6-31G(d), both positioned at 2.30 Å.

(II) The second hydrogen bond, between the hydrogen atom (H_{87}) and the lone pair oxygen atom (O_{148}) of the O_{11}-H_{87} bond, was positioned at 1.96 and 1.88 Å. The calculated H-bond energies were 8.50 (kcal mol^{-1}) (M08-HX/6-31G(d)) and 10.27 (kcal mol^{-1}) (PW6B95/6-31G(d)), respectively.

For orientation B. (I) The essential bond (O_{149}-H_{169}) and a hydrogen atom (H_{121}) were situated at 2.28 and 2.27 Å, respectively, with $E^{(2)}$ energies of 0.37 and 0.38 (kcal mol^{-1}) from M08-HX/6-31G(d) and PW6B95/6-31G(d), respectively.

(II) The second hydrogen bond was at 1.93 Å between the hydrogen atom (H_{147}) and the lone pair oxygen atom (O_{151}) in the O_{77}-H_{147} system. The calculated energy of this H-bond from

M08-HX/6-31G(d) was 5.25 (kcal mol^{-1}) (bond positioned at 1.92 Å, 6.60 (kcal mol^{-1}) from PW6B95/6-31G(d)).

In the case where HVA was acting as an acceptor; LP(O_{55}) and σ*(O_{149}-H_{169}) were at 1.83 and 1.84 Å, with energies of 3.83 and 15.99 (kcal mol^{-1}) from M08-HX/6-31G(d) and PW6B95/6-31G(d) in orientation A. Higher energy values of 22.72 and 27.96 (kcal mol^{-1}) were obtained for the interaction of the lone pair of LP(O_{11}) atom with the antibonding acceptor orbital σ*(O_{150}-H_{170}) in orientation B using M08-HX/6-31G(d) and PW6B95/6-31G(d), respectively.

According to NBO analysis, the compounds under study exhibited strong hyperconjugative interactions (LP (O_{55}) O_{149}-H_{169} and LP (O_{11}) O_{150}-H_{170}, respectively, for orientations A and B). The second-order energy $E^{(2)}$ was 15.99 and 27.96 kcal mol^{-1} at PW6B95/6-31G(d) level in the aqueous phase. The largest $E^{(2)}$ values were found in PW6B95/6-31G(d) in orientation B complex, as shown in Tables 6 and 7. The relationship between interaction energy and corresponding distances demonstrated that the higher the value of $E^{(2)}$, the shorter the interaction's contact distance.

^{1}H NMR Analysis

Using an equivalent TMS (tetramethylsilane) shielding estimated at the same theoretical levels as the reference, the GIAO approach was employed for ^{1}H NMR at the M08-HX/6-311+G(2d,p) and PW6B95/6-311+G(2d,p) density functional levels of theory [51]. NMR chemical shifts (δ) were calculated using the GIAO approach by subtracting the nuclear magnetic shielding tensors of the protons in the molecules of interest from those of TMS, serving as a reference, to provide results commensurate with experimental data. The polarizable continuum model (PCM) method was utilized to study the effects of the solvent (ε = 78.35), using water as a solvent.

$\delta = \sigma TMS - \sigma$

Table 8 and Fig. 8 present the outcomes of the experimental [42] and theoretical research. The estimated ^{1}H NMR chemical shifts of HVA in β-CD, including the inclusion complex's available experimental values (in ppm) with M08-HX/6-311+G(2d,p) and PW6B95/6-311+G(2d,p), are represented in Table 8. The proton signals of HVA, specifically H163, H164, and H165, showed notable chemical shift changes, while the other proton signals exhibited the least amount of chemical shift variation. Protons H161 and H164 from M08HX/6-311+G(2d,p) in orientation A showed the biggest difference between theoretical chemical shifts and observed chemical shifts in Table 8 and Fig. 8. Orientation A can be considered the most advantageous construction based on our theoretical findings.

Table 8. Calculation of Experimental and Theoretical ^{1}H NMR Chemical Shifts of the Inclusion Complex of HVA/β-CD at the M08HX/6-311+G(2d,p) and PW6B95/6-311+G(2d,p) Levels of the Theory for both Orientation

Protons	Experimental	Calculated			
	HVA in β-CD	M08HX		PW6B95	
		Orientation A	Orientation B	Orientation A	Orientation B
H_{161}	3.65	5.01	5.15	3.65	4.39
H_{162}	3.65	4.55	3.66	3.65	3.33
H_{163}	6.95	8.02	7.58	7.58	7.45
H_{164}	6.83	8.08	7.15	7.38	7.04
H_{165}	6.93	7.32	7.25	7.38	6.87
H_{166}	3.85	5.02	4.01	3.99	3.59
H_{167}	3.85	4.49	4.52	4.45	4.39
H_{168}	3.85	4.04	4.23	4.70	4.01
H_{169}	_	8.53	7.40	8.41	7.22
H_{170}	_	6.82	10.73	11.14	11.72

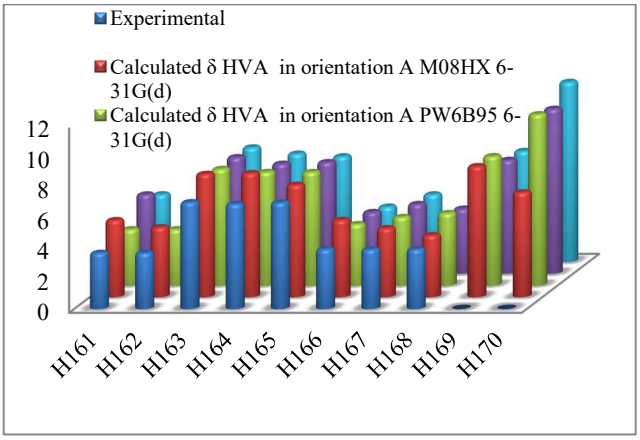

Fig. 8. Calculation of the inclusion complex of HVA/β-CD experimental and theoretical ^{1}H NMR chemical shifts for both orientations.

The results of the DFT combination computations using PW6B95/6-311+G(2d,p) are similar to the experimental results.

This analysis concludes that the PW6B95/6-311+G(2d,p) GIAO approach was justified in assigning all proton chemical shifts. To examine the relationship between theoretical and experimental NMR shielding tensors, the experimental data were plotted against the computed values from M08HX/6-311+G(2d,p) and PW6B95/6-311+G(2d,p) in orientation A. As depicted in Figs. 9 and 10, a strong linear correlation exists between the experimental and theoretical chemical shifts [52,53].

NCI-RDG Analysis

Weak intermolecular or intermolecular interactions can be elucidated through the analysis of reduced density gradient (RDG) calculations, providing insights into non-covalent interactions (NCI) that contribute to the stability of molecular

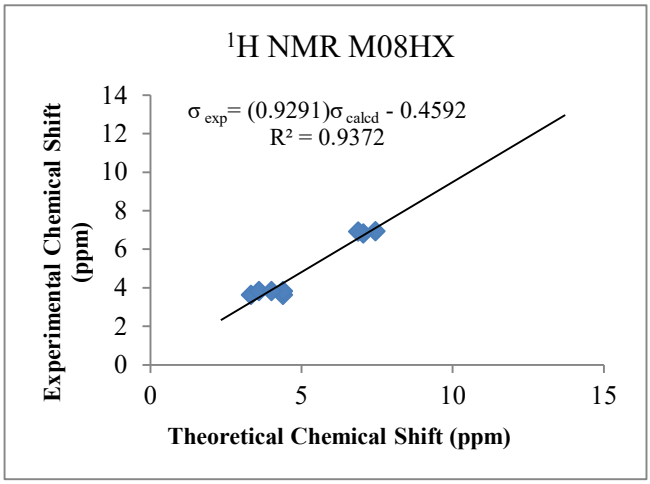

Fig. 9. A plot of experimental and theoretical ^{1}H NMR chemical shifts at the M08-HX/6-311+G(2d,p) level.

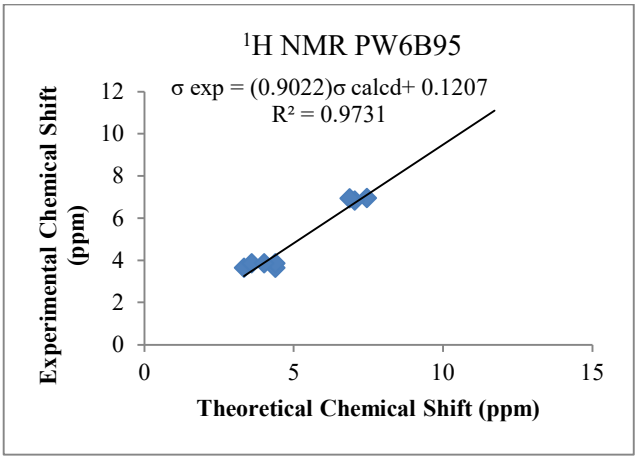

Fig. 10. A plot of experimental and theoretical ^{1}H NMR chemical shifts at the PW6B95/6-311+G(2d,p)) level.

structures [54]. The NCI-RDG analysis aims to characterize and interpret non-covalent interactions between HVA and β-CD. For all orientations, NCI-RDG analyses are presented in HVA/β-CD using an isosurface value of 0.5. The colors on the isosurfaces in Fig. 11 represent weak interactions, blue for strong attracting forces (van der Waals interactions), red for strong repulsive forces, and green (or earth green) for van der Waals interactions.

- Sign $(\lambda 2)\rho < 0$: Attractive interactions (van der Waals, hydrogen bonds)
- Sign $(\lambda 2)\rho > 0$: Repulsive interactions (steric crowding)

Bonds (shown in blue) between HVA and the hydrophobic interior cavity of the β-CD are clearly visible. Combining RDG and NCI research, it was demonstrated that while hydrogen bonds were weak and not visually apparent, van der Waals forces were the primary driving forces in the development of HVA/β-CD inclusion complexes (IC) (Fig. 9). These findings align with the molecular docking study's lowest binding affinity and RDG. Both van der Waals forces and hydrogen bonds contribute to the stability of the IC structure [55], as indicated by the NCI study based on the RDG, further confirming the development of the IC. Notably, the HVA/β-CD IC, the most stable among the three ICs, exhibited the densest distribution of van der Waals forces and hydrogen bonds. In orientation A, green patches indicative of hydrophobic interactions were observed between the primary hydroxyl and guest carboxyl functions (Fig. 11a). Direction B revealed forces between primary hydroxyl and OCH_3, as

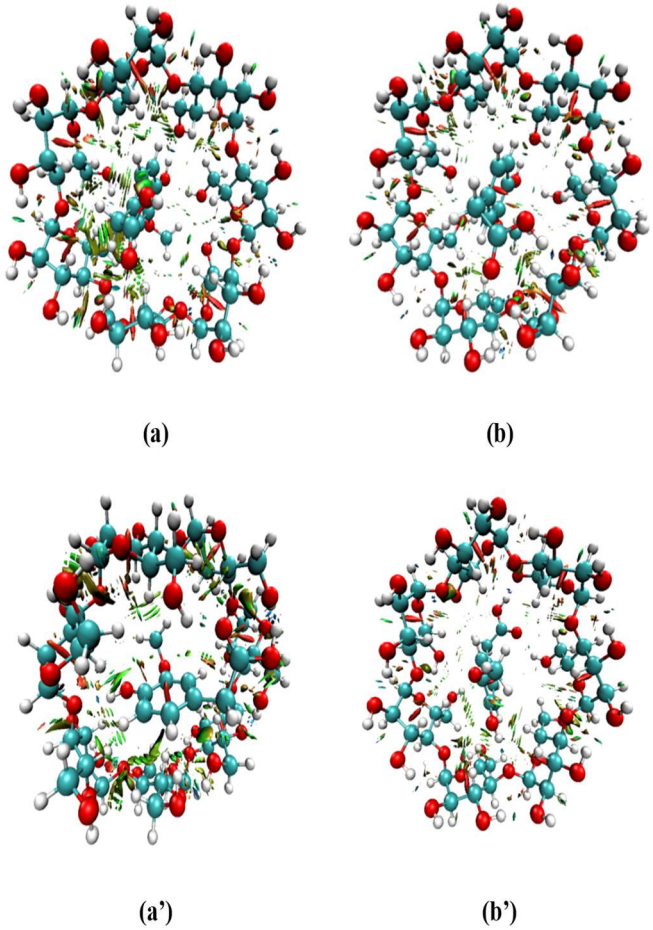

Fig. 11. The low-gradient isosurface of the HVA/β-CD in the M08HX and PW6B95 techniques in aqueous is present in both directions.

well as primary hydroxyl and guest alcohol functions. Additionally, red regions around the center of aromatic cycles indicated steric-repelling effects.

CONCLUSION

In this study, the interaction between β-CD and HVA was examined using three DFT functional levels-B3LYP, M08HX, and PW6B95-paired with a 6-31G(d) basis set. The investigation, conducted in both vacuum and aqueous environments, aimed to elucidate the complex dynamics of the formed complexes. Consistently, Orientation A emerged as the preferred configuration, demonstrating superior stability in both aqueous and vacuum conditions. The unique

confirmation adopted by HVA within the host cavity in vacuum underscored the robustness of this orientation. Moreover, complexation energy profiles highlighted the thermodynamic favorability of the host-guest interaction. Detailed analyses, including NBO simulations, emphasized the pivotal role played by intermolecular hydrogen interactions and Van der Waals forces in stabilizing the HVA/β-CD complexes. NBO and NCI analyses converged on the significance of Van der Waals forces as the principal driving force behind the complex formation. Comparative assessments of computational methods revealed the enhanced predictive accuracy of M08HX and PW6B95 in determining stable geometrical structures compared to the conventional B3LYP approach. The consistent encapsulation of HVA within the β-CD cavity further validated the reliability of these advanced methods. Notably, the PW6B95/6-311+G(2d,p) GIAO approach emerged as the most accurate in assigning proton chemical shifts, surpassing other methods utilized in this study.

Further research should refine computational methods, explore solvent effects, and consider temperature dependencies. Experimental validation and structural modifications can enhance specificity in interactions. Extended molecular dynamics simulations and exploration of potential applications offer promising avenues for HVA/β-CD complexes. These efforts aim to deepen insights and validate predictions.

REFERENCES

[1] Wimmer, T., Cyclodextrins. *Ullmann's Encyclopedia of Industrial Chemistry*. **2000**, 23-31, DOI: 10.1002/14356007.e08_e02.

[2] de Jesus, M. B.; Fraceto, L. F.; Martini, M. F.; Pickholz, M.; Ferreira, C. V.; de Paula, E., Non-inclusion complexes between riboflavin and cyclodextrins. *J. Pharm. Pharmacol.* **2012**, *64*, 832-842, DOI: 10.1111/j.2042-7158.2012.01492.x

[3] Nagatsu, T., The catecholamine system in health and disease-Relation to tyrosine 3-monooxygenase and other catecholamine-synthesizing enzymes-. *Proc. Jpn. Acad., Ser. B*. **2006**, *82*, DOI: 10.2183/pjab.82.388.

[4] Nichkova, M.; Wynveen, P. M.; Marc, D. T.; Huisman, H.; Kellermann, G. H., Validation of an ELISA for urinary dopamine: applications in monitoring treatment of dopamine-related disorders*., J. Neurochem.* **2013**, *125* (5), 724-735, DOI: 10.1111/jnc.12248.

[5] Okabe, N.; Hatanaka, Y.; Sasaki, Y., Structure of homovanillic acid. *Acta.Cryst. C.* **1991**, *47*, 2183-2185, DOI: 10.1107/S010827019100519X.

[6] Dong, Z.; Luo, Q.; Liu, J., Artificial enzymes based on supramolecular scaffolds. *Chem. Soc. Rev*. **2012**, *41*, 7890-7908, DOI: 10.1039/c2cs35207a.

[7] Al-Nouti, Y.; Bartlett, M. G., Comparison of local anesthetic-cyclodextrin non-covalent complexes using capillary electrophoresis and electrospray ionization mass spectrometry. *J. Am. Soc. Mass Spectrom*. **2002**, *13*, 928-935, DOI: 10.1016/S1044-0305(02)00395-1.

[8] Rao, K. R.; Nageswar, Y.; Krishnaveni, N. S.; Surendra, K., Supramolecular Catalysis of Organic Reactions Involving Cyclodextrins. *Advances in Organic Synthesis*. **2005**, *39*, 301-339, DOI: 10.2174/1574087054582969.

[9] Tafazzoli, M.; Ghiasi, M., Structure and conformation of α-, β-and γ-cyclodextrin in solution: Theoretical approaches and experimental validation. *Carbohydr. Polym*. **2009**, *78*, 10-15, DOI: 10.1016/j.carbpol.2009.02.020.

[10] Liu, L.; Guo, Q. -X., Use of quantum chemical methods to study cyclodextrin chemistry. *J. Incl. Phenom. Macrocycl. Chem*. **2004**, *50*, 95-103, DOI: 10.1007/s10847-003-8847-3.

[11] Dodziuk, H.; Lukin, O.; Nowiński, K., Molecular mechanics calculations of molecular and chiral recognition by cyclodextrins. Is it reliable? The selective complexation of decalins by β-cyclodextrin. *J. Mol. Struct*. **2000**, *503*, 221-230, DOI: 10.1016/S0166-1280(99)00299-7.

[12] Lambert, A.; Yeguas, V.; Monard, G.; Ruiz-López, M. F., What is the effective dielectric constant in a β-cyclodextrin cavity? Insights from Molecular Dynamics simulations and QM/MM calculations. *Comput. Theor. Chem*. **2011**, 968, 71-76, DOI: 10.1016/j.comptc.2011.05.008.

[13]Mazurek, A. H.; Szeleszczuk, Ł.; Gubica, T., Application of molecular dynamics simulations in the analysis of cyclodextrin complexes. *Int. J. Mol. Sci.* **2021**, *22* (17), 9422, DOI: 10.3390/ijms22179422.

[14] Yan, C.; Li, X.; Xiu, Z.; Hao, C., A quantum-mechanical study on the complexation of β-cyclodextrin with quercetin. *J. Mol. Struct.* ***2006****, 764,* 95-100, DOI : 10.1016/j.theochem.2006.02.008.

[15] Al-Sou'od, K. A., Molecular mechanics study of the inclusion complexes of some 1,2,4-oxadiazole derivatives of 3,3′-bis (1,2,4-oxadiazol-5 (4H)-one) with β-cyclodextrin. *J. Incl. Phenom. Macrocycl. Chem*. **2006**, *54*, 123-127, DOI: 10.1007/s10847-005-5237-z.

[16] Safia, H.; Ismahan, L.; Abdelkrim, G.; Mouna, C.; Leila, N.; Fatiha, M., Density functional theories study of the interactions between host β-Cyclodextrin and guest 8-Anilinonaphthalene-1-sulfonate: Molecular structure, HOMO, LUMO, NBO, QTAIM and NMR analyses. *J. Mol. Liq*. **2019,** ***280***, 218-229, DOI: 10.1016/j.molliq.2019.01.019.

[17] Zhao, Y.; Truhlar, D. G., Exploring the limit of accuracy of the global hybrid meta density functional for main-group thermochemistry, kinetics, and noncovalent interactions. *J. Chem. Theory. Comput*. **2008**, *4*, 1849-1868, DOI: 10.1021/ct800246v.

[18] Jenita, M. J., Prabhu, A., Rajendiran, N., Theoretical study of inclusion complexation of tricylic antidepressant drugs with β-cyclodextrin. *Indian. J. Chem*. **2012**, *51A*, 1686-1694.

[19] Rafati, A.; Hashemianzadeh, S.; Nojini, Z.; Safarpour, M., Theoretical study of the inclusion complexes of α and β-cyclodextrins with decyltrimethylammonium bromide (DTAB) and tetradecyltrimethylammonium bromide (TTAB). *Mol. Liq*. **2007**, *135*, 153-157, DOI: 10.1016/j.molliq.2006.11.006.

[20] Haoyu, S. Y.; He, X.; Li, S. L.; Truhlar, D. G., MN15: A Kohn-Sham global-hybrid exchange-correlation density functional with broad accuracy for multi-reference and single-reference systems and noncovalent interactions. *Chem. Sci*. **2016**, *7*, 5032, DOI: 10.1039/c6sc00705h.

[21] Zhao, Y.; Truhlar, D. G., Design of density functionals that are broadly accurate for thermochemistry, thermochemical kinetics, and nonbonded interactions. *J. Phys. Chem*. *A* **2005**, *109*, 5656-5667, DOI: 10.1021/jp050536c.

[22] Bolton, E. E.; Wang, Y.; Thiessen, P. A.; Bryant, S. H., PubChem: integrated platform of small molecules and biological activities. *Annual Reports in Computational Chemistry, 4, Elsevier*. **2008**, *4*, 217-241, DOI: 10.1016/S1574-1400(08)00012-1.

[23] Rajkumar, P.; Selvaraj, S.; Anthoniammal, P.; Kumar, A. R.; Kasthuri, K.; Kumaresan, S., Structural (monomer and dimer), spectroscopic (FT-IR, FT-Raman, UV-Vis and NMR) and solvent effect (polar and nonpolar) studies of 2-methoxy-4-vinyl phenol. *Chemical Physics Impact*. **2023**, *7*, 100-257, DOI: 10.1016/j.chphi.2023.100257.

[24] Selvaraj, S., I*n silico* studies on the molecular geometry, FMO, mulliken charges, MESP, ADME and molecular docking prediction of pyrogallol carboxaldehydes as potential anti-tumour agents. *Phys. Chem. Res*. **2023**, *12*, 2, 305-320, DOI: 10.22036/PCR.2023.402835.2359.

[25] Hehre, W. J.; Ditchfield, R.; Pople, J. A., Self-consistent molecular orbital methods. XII. Further extensions of Gaussian-type basis sets for use in molecular orbital studies of organic molecules. *J. Chem. Phys*. **1972**, 56, 5, 2257-2261, DOI: 10.1063/1.1677527.

[26] Cheeseman, J. R.; Trucks, G. W.; Keith, T. A.; Frisch, M. J., A comparison of models for calculating nuclear magnetic resonance shielding tensors. *J. Chem. Phys*. **1996**, *104*, 5497-5509, DOI: 10.1063/1.471789.

[27] Kim, S.; Chen, J.; Cheng, T.; Gindulyte, A.; He, J.; He, S., *et al*., PubChem 2019 update: improved access to chemical data. Nucleic acids research. **2019**, *47*, D1102-D9.

[28] Frisch, M. E.; Trucks, G.; Schlegel, H.; Scuseria, G.; Robb, M.; Cheeseman, J., *et al*., Gaussian 16, revision C. 01. Gaussian, Inc., Wallingford CT, **2016**.

[29] Bounab, M. M.; Stephane, H.; Djémil, R.; Fatiha, M.; Leila, N., Molecular dynamics and quantum mechanics study of the [2-oxo-N-phenyl-3-oxazolidinesulfonamide@β-cyclodextrin] complex. *J. Mol. Liq*. **2006**, *222*, 777-782, DOI: 10.1016/j.molliq.2016.07.121.

[30] Rahim, M.; Madi, F.; Nouar, L.; Bouhadiba, A.; Haiahem, S.; Khatmi, D. E. *et al*., Driving forces and electronic structure in β-cyclodextrin/3,3′-diaminodiphenylsulphone complex. *J. Mol. Liq*. **2014**, *199*, 501-510, DOI: 10.1016/j.molliq.2014.09.035.

[31] Hyperchem, R., 7.51 for windows 2002 Hypercube. Inc,

Gainesville, **2002**.

[32] Millam, J.; Dennington, R.; Keith, T., GaussView Version 5. Semichem, Inc: Shawnee Mission, KS, **2009**.

[33] de Sousa, S. M. R.; Guimarães, L.; Ferrari, J. L.; De Almeida, W. B.; Nascimento Jr, C. S., A DFT investigation on the host/guest inclusion process of prilocaine into β-cyclodextrin. *Chem. Phys. Lett*. **2016**, *652*, 123-129, DOI: 10.1016/j.cplett.2016.04.053.

[34] Guendouzi, A.; Mekelleche, S. M.; Brahim, H.; Litim, K., Quantitative conformational stability host-guest complex of Carvacrol and Thymol with β-cyclodextrin: a theoretical investigation. *J. Incl. Phenom. Macrocycl. Chem*. **2017**, *89*, 143-155, DOI: 10.1007/s10847-017-0740-6.

[35] Djilani, I.; Madi, F.; Nouar, L.; Haiahem, S.; Rahim, M.; Khatmi, D. E., *et al*., Theoretical investigation to characterize the inclusion complex of α-lipoic acid and β-cyclodextrin. *C. R. Chim*. **2015**, 18, 170-177, DOI: 10.1016/j.crci.2014.05.003.

[36] Leila, N.; Sakina, H.; Bouhadiba, A.; Fatiha, M.; Leila, L., Molecular modeling investigation of *para*-nitrobenzoic acid interaction in β-cyclodextrin. *J. Mol. Liq*. **2011**, *160*, 1-7, DOI: 10.1016/j.molliq.2011.02.004.

[37] Attoui Yahia, H.; Attoui Yahia, O.; Khatmi, D.; Belghiche, R.; Bouzitouna, A., Quantum chemical investigations on hydrogen bonding interactions established in the inclusion complex β-cyclodextrin/benzocaine through the DFT, AIM and NBO approaches. *J. Incl. Phenom. Macrocycl. Chem.* **2017**, *89*, 353-365, DOI:10.1007/s10847-017-0753-1.

[38] Wagner, B. D.; Fitzpatrick, S. J., A comparison of the host-guest inclusion complexes of 1, 8-ANS and 2, 6-ANS in parent and modified cyclodextrins. *J. Incl. Phenom. Macrocycl. Chem*. **2000**, *38*, 467-478, DOI: 10.1023/A:1008198825835.

[39] Sueishi, Y.; Fujita, T.; Nakatani, S.; Inazumi, N.; Osawa, Y., The enhancement of fluorescence quantum yields of anilino naphthalene sulfonic acids by inclusion of various cyclodextrins and cucurbit [7] uril. *Spectrochim. Acta* .**2013**, *114*, 344-349, DOI: 10.1016/j.saa.2013.05.052.

[40] Meryem, G.; Rabah, K.; Fatiha, M.; Leila, N.; Aziz, B. A.; Imane, D.; *et al*., Computational investigation of vanillin@*βéta*-cyclodextrin inclusion complex: Electronic and intermolecular analysis. *J. Mol. Liq*. **2021**, *321*, *11*, 4839, DOI: 10.1016/j.molliq.2020.114839.

[41] Hadjer, N.; Tahar, A.; Brahim, H.; Abdelkrim, G.; Didier, V., Theoretical Investigation on Inclusion Complex of (s)-2-Isopropyl-1-(o-nitrophenyl) Sulfonyl) Aziridine with β-Cyclodextrin. *Phys. Chem. Res*. **2022**, *10*(1), 69-87, DOI: 10.22036/pcr.2021.288704.1920.

[42] Korytkowska-Wałach, A.; Dubrawska, B.; Śmiga-Matuszowicz, M.; Bieg, T., Spectroscopic study on the inclusion complexes of β-cyclodextrin with selected metabolites of catecholamines. *J. Mol. Str*. **2017**, *1127*, 532-538, DOI: 10.1016/j.molstruc.2016.08.010.

[43] Suvitha, A.; Venkataramanan, N. S.; Mizuseki, H.; Kawazoe, Y.; Ohuchi, N., Theoretical insights into the formation, structure, and electronic properties of anticancer oxaliplatin drug and cucurbit [n] urils n = 5 to 8. *J. Incl. Phenom. Macrocycl. Chem.* **2010**, *66*, 213-218, DOI: 10.1007/s10847-009-9601-2.

[44] Siva, S.; Thulasidhasan, J.; Rajendiran, N., Host-guest inclusion complex of propafenone hydrochloride with α-and β-cyclodextrins: Spectral and molecular modeling studies. *Spectrochim. Acta A*. **2013**, *115*, 559-567, DOI: 10.1016/j.saa.2013.06.079.

[45] Sugimori, K.; Shuku, T.; Sugiyama, A.; Nagao, H.; Sakurai, T.; Nishikawa, K., Solvent effects on electronic structure of active site of azurin by polarizable continuum model. *Polyhedron*. **2005**, *24*, 2671-2675, DOI: 10.1016/j.poly.2005.03.140.

[46] Tamer, Ö.; Avcı, D.; Atalay, Y., Calculations of electronic structure and nonlinear optical parameters of 4-methoxybenzaldehyde-N-methyl-4-stilbazolium tosylate. *J. Appl.Spectrosc*. **2014**, *80*, 971-982, DOI: 10.1007/s10812-014-9875-z.

[47] Mulliken, R. S., Electronic population analysis on LCAO-MO molecular wave functions. *I, J. Chem. Phys.*, **1955**, *23*, 1833-1840, DOI: 10.1063/1.1740588.

[48] Yüksek, H.; Cakmak, I.; Sadi, S.; Alkan, M.; Baykara, H., Synthesis and GIAO NMR Calculations for Some Novel 4-Heteroarylidenamino-4,5-dihydro-1H-1,2,4-triazol-5-one Derivatives: Comparison of Theoretical and Experimental 1H-and 13C-Chemical Shifts. *Int. J.*

Mol. Sci. **2005**, *6*, 219, DOI: 10.3390/i6060219.

[49] Ram Kumar, A.; Selvaraj, S.; Azam, M.; Sheeja Mol, G.; Kanagathara, N.; Alam, M., *et al*., Spectroscopic, biological, and topological insights on lemonol as a potential anticancer agent. *ACS Omega.* **2023**, *8*, 34, 31548-31566, DOI: 10.1021/acsomega.3c04922.

[50] Kumar, A. R.; Selvaraj, S.; Anthoniammal, P.; Ramalingam, R. J.; Balu, R.; Jayaprakash, P., *et al*., Comparison of spectroscopic, structural, and molecular docking studies of 5-nitro-2-fluoroaniline and 2-nitro-5-fluoroaniline: An attempt on fluoroaniline isomers. *Journal of Fluorine Chemistry.* **2023***, 270*, 110167, DOI: 10.1016/j.jfluchem.2023.110167.

[51] Bouhadiba, A.; Belhocine, Y.; Rahim, M.; Djilani, I.; Nouar, L.; Khatmi, D. E., Host-guest interaction between tyrosine and β-cyclodextrin: Molecular modeling and nuclear studies. *J. Incl. Phenom. Macro Chem*. **2013**, *76*, 379-384, DOI: 10.1016/ j.molliq.2017.03.029.

[52] Sheikhshoaie, I.; Saheb, V., A new salen base 5-(phenylazo)-N-(2-amino pyridine) salicyliden Schiff base ligand: Synthesis, experimental and density functional studies on its crystal structure, FTIR, ^{1}H NMR and ^{13}C NMR spectra. *Spectrochimica Acta*. **2010**, *77*, 1069-1076, DOI: 10.1016/j.saa.2010.08.075.

[53] Saheb, V.; Sheikhshoaie, I., A new Schiff base compound N,N′-(2,2-dimetylpropane)-bis (dihydroxylacetophenone): Synthesis, experimental and theoretical studies on its crystal structure, FTIR, UV-visible, ^{1}H NMR and ^{13}C NMR spectra. *Spectrochimica. Acta. Part* A. **2011**, *81*, 144-150, DOI: 10.1016/j.saa.2011.05.080.

[54] de Assis, J. V.; Teixeira, M. G.; Soares, C. G.; Lopes, J. F.; Carvalho, G. S.; Lourenço, M. C., *et al.* ,Experimental and theoretical NMR determination of isoniazid and sodium p-sulfonatocalix [n] arenes inclusion complexes. *Eur. J. Pharmaceut. Sci*. **2012**, *47*, 539-548, DOI: 10.1016/j.ejps.2012.07.015.

[55] Arruda, T. R.; Marques, C. S.; Soares, N. F. F., Native Cyclodextrins and Their Derivatives as Potential Additives for Food Packaging: A Review. *Polysaccharides*. **2021**, *2*, 825-842, DOI: 10.3390/ polysaccharides2040050.